

Paper to appear in Nature Materials, accepted 26 Sept 2007.

Lattice dynamics of the Zn-Mg-Sc icosahedral quasicrystal and its Zn-Sc periodic 1/1 approximant.

Marc de Boissieu^{1**}, Sonia Francoual^{1,2*}, Marek Mihalkovič^{3,1}, Kaoru Shibata⁴, Alfred Q.R. Baron^{5,6}, Yvan Sidis⁷, Tsutomu Ishimasa⁸, Dongmei Wu⁹, Thomas Lograsso⁹, Louis-Pierre Regnault¹⁰, Franz Gähler¹¹, Satoshi Tsutsui⁶, Bernard Hennion⁷, Pierre Bastie^{12,2}, Taku J. Sato¹³, Hiroyuki Takakura⁸, Roland Currat², An-Pang Tsai¹⁴

1- Sciences et Ingénierie des Matériaux et Procédés, INPGrenoble CNRS UJF, BP 75 38402 St Martin d'Hères Cedex, France

2- Institut Laue Langevin, BP 156, 38042 Grenoble, Cedex 9, France

3- Institute of Physics, Slovak Academy of Sciences, 84228 Bratislava, Slovakia.

4- J-PARC Center, Japan Atomic Energy Agency, 2-4, Shirakatashirane, Tokai, Naka, Ibaraki 319-1195, Japan

5- RIKEN/SPring-8, 1-1-1 Kouto, Sayo, Hyogo 679-5143, Japan

6- JASRI/SPring-8, 1-1-1 Kouto, Sayo, Hyogo 679-5198, Japan

7- Laboratoire Léon Brillouin, CEA Saclay, 91191 Gif sur Yvette Cedex, France

8- Division of applied Physics, graduate school of engineering, Hokkaido University, Sapporo, 060-8628 Japan

9- Ames Laboratory, Iowa State University, Ames, Iowa 50011, USA

10- CEA-grenoble, DRFMC-SPSMS-MDN, 38054 Grenoble cedex 9, France

11- Institut für Theoretische und Angewandte Physik, Universität Stuttgart, Pfaffenwaldring 57, 70550 Stuttgart, Germany

12- Laboratoire de Spectrométrie Physique, Université Joseph Fourier, BP 87, 38402 St Martin d'Hères Cedex, France

13- Neutron Science Laboratory, Institute for Solid State Physics, University of Tokyo, 106-1 Shirakata, Tokai, Ibaraki 319-1106, Japan

14- Institute of Multidisciplinary Research for Advanced Materials, Tohoku University, Sendai 980-8577, Japan

15- National Institute for Material Science, Tsukuba 305-0044, Japan

* present address: National High Magnetic Field Laboratory, Los Alamos National Laboratory, MPA - NHMFL, TA-35, Bldg. 0127, MS E536, Los Alamos, New Mexico 87545, USA

** corresponding author : Marc.de-boissieu@ltpcm.inpg.fr

Abstract:

Quasicrystals are long range ordered materials which lack translational invariance so that the study of their physical properties remains a challenging problem. In order to study the respective influence of the local order and of the long range order (periodic or quasiperiodic)

on lattice dynamics, we have carried out inelastic x-ray and neutron scattering experiments on single grain samples of the Zn-Mg-Sc icosahedral quasicrystal and of the Zn-Sc periodic cubic 1/1 approximant. Besides the overall similarities and the existence of a pseudo gap in the transverse dispersion relation, marked differences are observed, the pseudo gap being larger and better defined in the approximant than in the quasicrystal. This can be qualitatively explained using the concept of pseudo Brillouin zone in the quasicrystal. These results are compared to simulations on atomic models and using oscillating pair potentials. The simulations reproduce in details the experimental results.

Quasicrystals¹ are long range ordered structures which lack lattice periodicity. Although progress has been made in deciphering their atomic structure the understanding of their physical properties remains a challenging and fascinating problem since the Bloch theorem can no longer be applied. The stable binary i-Cd-Yb² icosahedral (i-) phase and the isostructural i-Zn-Mg-Sc³ phase are particularly interesting in that respect since both a quasicrystal and a periodic approximant can be synthesised, with almost the same chemical composition^{4,5}. As shown recently⁶, their structure can be described by a packing of a large rhombic triacontahedral (RTH) unit with a diameter of about 1.52 nm and containing about 158 atoms arranged on successive shells (Figure 1). In both the quasicrystal (QC hereafter) and the 1/1 approximant the RTH units are connected along their 2-fold axes by shared faces, and along their 3-fold axes where they overlap. In the 1/1 approximant the RTH are located on the vertices of a BCC lattice (lattice parameter $a=1.57$ and 1.38 nm for CdYb and ZnSc respectively). In the QC 94% of the atoms are part of the RTH units which are located on vertices of a quasiperiodic network, with two small structural units filling the gaps between the clusters. The QC and its approximant thus offer a unique possibility of comparing the respective effect of the short range order (RTH units) and long range order (periodic versus quasiperiodic) on physical properties and on their lattice dynamics.

Exact calculation of physical properties and lattice dynamics have only been carried out in 1D systems (see references^{7,8} for an introduction). The most striking result for electronic or vibrational states is the existence of critical modes which are neither extended as in periodic structures, nor localised as in disordered systems. Although simulations on large periodic approximant have been carried out in 2D and 3D, whether critical modes, with the characteristic power law decay of the wavefunction or eigenmodes, exist in 3D systems is still an open question. Recent experimental comparison of the thermal, electric transport properties⁹⁻¹² and of the electronic structure^{13,14} of the i-CdYb or i-ZnMgSc QC and their 1/1 approximants showed only minor differences, and/or an effect of chemical disorder¹⁵, so that a clear signature of the quasiperiodicity on physical properties remains to be evidenced.

To tackle this problem we have undertaken a detailed comparative study of the lattice dynamics of the icosahedral quasicrystalline phase and its 1/1 approximant in the ZnSc system by means of inelastic neutron and x-ray scattering on single grains samples. These are very sensitive spectroscopic tools probing the inelastic response function $S(\mathbf{Q}, E)$, which is related to the space and time Fourier transform of the structure. We show that the inelastic response function of both the QC and the approximant do present an extremely rich structure, with a pseudo gap between an optical and a transverse acoustic branch. We also observe marked differences which can be qualitatively explained using the concept of pseudo Brillouin zones in the QC.

We have compared these results with atomic scale simulations. This is a difficult problem which could be overcome only because (i) a detailed knowledge of the atomic structure of the QC and its approximant is now available, (ii) oscillating pair potentials have been fitted against ab-initio data¹⁶ allowing to handle with systems of several thousands of atoms. We demonstrate that the simulations reproduces both the experimental dispersion relations and the intensity distribution of the response function $S(\mathbf{Q}, E)$, which is a much severe test. Using a complete set of experimental data and atomistic simulations we have thus achieved the first

detailed comparison between model and experiment of the lattice dynamics of a quasicrystal and its 1/1 approximant.

Single grain samples of the $i\text{-Zn}_{80.5}\text{Mg}_4\text{Sc}_{15.5}$ quasicrystalline phase and the 1/1 $\text{Zn}_{85.5}\text{Sc}_{14.5}$ cubic approximant have been prepared by slow cooling from the melt. The icosahedral quasicrystal is of high structural quality as shown by its small mosaic spread and the small amount of phason diffuse scattering in its diffraction pattern¹⁷. As a consequence of both, atomic size differences and electronic hybridisation, the quasicrystal is very well ordered chemically¹⁸.

The inelastic response function $S(\mathbf{Q}, E)$ has been measured by inelastic neutron and x-ray scattering (see methods). Unlike the case of a crystal, for QC the wavevector \mathbf{q} is no longer a good quantum number and is ill defined. However both simulations and experiments (see¹⁹ for a review) have demonstrated that strong Bragg peaks can be chosen as zone centre with the response function written as $S(\mathbf{Q}_{\text{Bragg}} + \mathbf{q}, E)$, where $\mathbf{Q}_{\text{Bragg}}$ is a reciprocal lattice vector. Moreover around each zone centre one can define pseudo Brillouin zone boundary (PBZB) within a weak coupling type theory¹⁹⁻²³ (see supplementary information). This was confirmed by previous experimental results on icosahedral phases, where for \mathbf{q} smaller than 0.5 \AA^{-1} well defined acoustic modes are observed whereas for higher wavevectors, the response function is characterised by a series of broad dispersionless optic-like modes²⁴⁻²⁸. The crossover between the two regimes is abrupt and occurs for a wavelength in the range of 20 to 10 \AA (or a wavevector of the order $0.3\text{-}0.6 \text{ \AA}^{-1}$) while the acoustic mode broadens rapidly likely as a consequence of a mixing with the lower optic-like excitations²⁹.

Within the above approximation we present hereafter the dispersion relations. We also focus on the intensity distribution of the $S(\mathbf{Q}, E)$ function which is related to the pattern of atomic displacements.

We first present experimental results obtained in transverse geometry. Constant- \mathbf{Q} energy scans were measured by inelastic neutron scattering around the strong 2-fold reflection lying on the (1,0,0) axis, with N/M indices³⁰ 52/84 for the QC ($Q_{\text{Bragg}}=4.48 \text{ \AA}^{-1}$) and (10 0 0) for the 1/1 approximant ($Q_{\text{Bragg}}=4.53 \text{ \AA}^{-1}$). These reflections are chosen as zone centre, and the wavevector \mathbf{q} is parallel to (0,1,0) direction (Fig. 1). Fig. 2 displays the measured intensity distribution shown as a colour scale together with the extracted dispersion relation shown as symbols. For the sake of clarity only the low energy part ($E < 15 \text{ meV}$) of the spectrum is shown. A few individual scans are displayed in Fig. 5, left panels.

A well-defined transverse acoustic mode is observed for both the QC and the approximant near the zone centre, as illustrated by the two scans at $q=0.18 \text{ \AA}^{-1}$ in the Fig 5 (two left panels). Its width remains resolution limited up to $q=0.3 \text{ \AA}^{-1}$ and it exhibits a linear dispersion from which we determine a transverse acoustic (TA) sound velocity of $2670 (\pm 30)$ and $2660 (\pm 30) \text{ ms}^{-1}$ for the QC and the 1/1 approximant respectively. The linear dispersion is shown as a solid line in Fig. 2. Whereas the TA dispersion is found to be isotropic in the QC a weak anisotropy is observed in the 1/1 approximant. For both the QC and the 1/1 approximant the acoustic excitation broadens rapidly for q wavevectors between 0.3 \AA^{-1} and 0.6 \AA^{-1} , to reach a width of 2 meV FWHM, as illustrated by the scans at $q=0.54$ and 0.53 \AA^{-1} in Fig. 5. Along with the broadening the dispersion departs from linearity (Fig 2) and the normalised inelastic intensity (see methods) increases, indicating that there is a mode mixing (this is shown as

triangles on the Fig 2). An optical excitation is observed a higher energy, centred at 13 ± 0.3 meV in the 1/1 approximant and 12.3 ± 0.3 meV in the QC. This excitation is rather broad (about 3 to 4 meV FWHM) but is well defined, and a pseudo gap separates it from the acoustic excitation (Fig 2 and 5). The optical mode intensity increases as q increases away from the zone centre, so that for $q > 0.7\text{\AA}^{-1}$ its intensity becomes larger than the one of the acoustic mode (see Fig 2 and 5). Although this trend is better seen in the approximant, it is also observed in the quasicrystal, with a rather standard scenario in which the intensity is ‘transferred’ from the acoustic mode to the optical one, as expected close to a zone boundary.

There are two marked differences distinguishing the response function of the QC from its approximant. (i) The pseudo gap between the optic and acoustic excitation is significantly larger in the 1/1 approximant than in the QC, about 3 meV instead of 2 meV (see Figure 2). (ii) For q smaller than 0.4\AA^{-1} an optical excitation located at 7.5 meV is observed in the approximant only. It crosses the acoustic one at the first BZB, where the acoustic signal is already significantly broadened and can thus be interpreted as resulting from a gap opening at the BZB.

Differences can be qualitatively explained using the concept of pseudo Brillouin zone in the QC. The first BZB of the 1/1 approximant, located at 0.45\AA^{-1} , is replaced by two consecutive PBZB located at 0.33\AA^{-1} and 0.53\AA^{-1} associated with the 4/0 and 4/4 2-fold axis reflections (Figure 2) and having a smaller associated Fourier component (see supplementary information). One thus expects a weaker Bragg plane reflection in the QC than in the approximant. This qualitatively explains why the 7.5 meV mode only shows up in the 1/1 approximant. The larger number of PBZB as compared to BZB makes them also less effective and explains the smaller observed pseudo-gap in the QC. Moreover, the larger number of optical modes in the QC will ‘fill’ the pseudo gaps. Such an effect is for instance observed in simulations on the Fibonacci chain and its approximant^{19,31}.

Similar observations have been made for longitudinal excitations measured by inelastic X-ray scattering. Figure 3 displays the dispersion relation extracted from constant- \mathbf{Q} energy scans measured in both the approximant and the QC around the strong 2-fold Bragg reflection 52/84 or (10 0 0), some characteristic scans being shown Fig. 5, right panel. As for transverse excitations, special PBZB and zone boundaries are shown as vertical dashed lines. Again, the two dispersion relations are similar in the QC and the approximant. The LA sound velocities are found to be equal to $4910\pm 200\text{ ms}^{-1}$, in both the QC and the approximant. Longitudinal acoustic modes are well defined only for wavevectors smaller than 0.25\AA^{-1} , above which the dispersion relation starts to bend over together with a rapid broadening of the acoustic signal. A well defined dispersionless optical excitation is observed at 15.8 ± 0.6 meV in the approximant and 14.8 ± 0.6 meV in the quasicrystal (see red arrows in Fig. 5). As in the transverse geometry case, this optical excitation sits at a smaller energy in the QC. We also observe a low lying optical excitation at about 5.9 ± 0.6 and 6.6 ± 0.6 meV in the QC and the approximant respectively. This mode displays a strong intensity variation and is particularly visible for positive phonon wavevector \mathbf{q} (*i.e.* for $\mathbf{Q}=\mathbf{Q}_{\text{Br}}+\mathbf{q}$ larger than 4.5\AA^{-1}). This is particularly visible in Fig. 5 (right panels), the intensity of the mode at 6 meV being much weaker for $q=-0.45\text{\AA}^{-1}$ than for $q=0.45\text{\AA}^{-1}$ (note that the intensity scale is different in the two panels). At higher energy, broad and dispersion-less excitations are also observed at around

20 and 28 meV in the QC and the approximant, the energy positions being always slightly lower in the QC.

As for transverse modes, the marked differences between the QC and the approximant show up mainly around the Brillouin and pseudo Brillouin zone boundaries. The single zone boundary in the approximant is replaced by 2 PBZB in the QC. As a result the pseudo gap opening is better seen in the approximant whereas in the QC we mainly observe a signal broadening, as is visible around $q=-0.45 \text{ \AA}^{-1}$.

The above experimental results have been compared with simulations on realistic atomic models. To model the interactions in the Zn-Sc system, we used oscillating pair potentials which have been fitted against ab-initio data (see methods)¹⁶ and are shown Figure 6.

A difficulty encountered in the modelling of the 1/1 approximant and the quasicrystal is the orientational correlations of the central tetrahedra of the atomic cluster (see Fig. 1). Indeed in the 1/1 approximant whereas tetrahedra have a disordered orientations at room temperature, an ordering takes place below 150K leading to a superstructure^{32 33}. Structural analysis of the 1/1 ordered low T phase showed that the tetrahedron orientation induces a strong distortion of the successive icosahedral shells, breaking their icosahedral symmetry³³. To model the room-temperature random tetrahedron orientations, we took a larger supercell containing 8 clusters and with lattice parameters equal to $a_1=2a$, $b_1=c_1=\sqrt{2}a$, where a is the lattice parameter of the 1/1 approximant and equals to 13.76 \AA . We positioned tetrahedra randomly at each of its 8 cluster centres, then performed molecular dynamics annealing of the structure at room temperature, followed by quench to $T=0\text{K}$. We have found that introducing this disorder is crucial in order to have a reasonable comparison with experimental data (see supplementary information).

To compute the dynamical response of the QC, we needed a unique realization of the structure with periodic boundary condition. We used a 3/2 cubic approximant which contains 32 clusters in the unit cell, and has lattice parameter equal to 36.13 \AA . We considered a binary decoration Zn-Sc, based on the related i-CdYb atomic structure⁶ and on the ternary 2/1 MgScZn³⁴. The modelling was achieved by positioning the RTH units on the vertices of the so called canonical cell tiling³⁵ of the 3/2 approximant with a decoration procedure as described in³⁶. Ambiguous atomic sites positions were determined by total energy minimisation. As for the 1/1 approximant, the tetrahedral orientation where obtained by a molecular dynamic annealing followed by a quench. Induced deviations from icosahedral symmetry of the successive shells around the tetrahedron are, as for the 1/1 approximant, a crucial parameter (see arrows in Fig 1). The resulting model has a composition $\text{Zn}_{2528}\text{Sc}_{456}$, contains 2984 atoms per unit cell and presents a diffraction pattern which compares well to the QC one (see supplementary information).

Using these models and the fitted pair potentials the inelastic response function $S(\mathbf{Q},E)$ has been calculated either in the harmonic approximation and by direct diagonalisation of the dynamical matrix, or from atom trajectories generated by room temperature molecular dynamics, using the method described in ref.³⁷. The latter approach is not relying on the harmonic approximation, which might have been an issue due to suspected shallow minima in the energy landscape related to tetrahedron librations. However, the two approaches did not

show any significant differences wherefore in this paper we only report dynamical matrix results.

Figures 3 and 4 display the calculated $S(\mathbf{Q},E)$ in the longitudinal and transverse geometry for both the approximant and the quasicrystal. The calculation is temperature colour coded, and does not include the term $n(E)/E$ (where $n(E)$ is the Bose occupation factor), so that the acoustic mode presents a constant intensity. In both figures, the simulation has been convoluted with a Gaussian distribution with FWHM of 1 meV. Although the calculated transverse acoustic excitations are slightly too soft, the main features are nicely reproduced by the calculation: acoustic modes and pseudo gap, high energy optical excitations, low lying optical excitation in longitudinal geometry. Even the detailed differences between the QC and the approximant are reproduced: a larger pseudogap in the approximant than in the QC, the interaction with an optical excitation around 7.5 meV at the BZB in transverse geometry for the approximant, lower positions of the optical bands in the QC than in the approximant.

Not only the dispersion relations are matched by the calculation, but also the intensity distribution is qualitatively well reproduced (compare Fig 2 and 4). To illustrate this point, simulated spectra have been superimposed on the experimental data for a few characteristic scans in Fig. 5. Neutron and X-ray simulated spectra have been convoluted with a Gaussian distribution (1 and 3 meV FWHM respectively), to account for the effect of instrumental resolution. Although transverse modes are too soft, the intensity distribution is well reproduced by the calculation. In particular, the larger gap observed in the approximant is well accounted for. The broadening of TA mode is also well reproduced, demonstrating that it corresponds to mixing with low lying excitations, since the simulation is carried out in the harmonic approximation. For longitudinal excitations, the intensity distribution is also well reproduced. Note in particular the good reproduction of the different intensity distribution at $+$ and -0.45 \AA^{-1} for the mode located at 6 meV (Figure 5).

Note that the overall intensity scale factor in the simulation has been found to be q dependant, which might be partly due to experimental difficulties, but also points towards some of the limitations of the simulation. Nevertheless we emphasize that this detailed semi-quantitative comparison is a very severe test for both the atomic model and the pair potentials used. The overall good agreement between calculation and observation thus opens the route for a further and detailed analysis of the vibrational modes in the system on a firmly established model. This is underway and we point to some questions which can be now tackled: do the clusters play a significant role in the vibrational properties as suggested in^{38,39}, does the hierarchical packing of clusters (see Fig. 5 of ref⁶) play a role as proposed in^{38,40}?, are they critical modes?, are the low lying longitudinal modes related to the inner tetrahedron motion?

Besides the field of QC and complex metallic alloys, there are two other research fields where our results might be of interest. The first is the one of photonic⁴¹ or more recently phononic band gap quasicrystal⁴² which have been suggested to be more efficient at a total band gap opening than their periodic counterpart because of the high symmetry of the pseudo Brillouin zone. Our results suggest that a 1/1 type approximant might be better suited than QC arrangements, because the Bragg plane reflections is more efficient than in the QC state. This of course strongly depends on the wave vector and the Fourier component of the Bragg plane responsible for the gap opening. The second field is thermoelectrics, for which a poor phonon

heat transport or phonon glass-like state is a crucial parameter⁴³. Most quasicrystals have been found to be poor thermal conductors^{10,44,45} which has been attributed to a generalised umklapp process⁴⁶ or to a hierarchically variable range hopping on clusters⁴⁰. The present simulations and results show that there is a strong acoustic-optic mode mixing for wavevectors larger than 0.3 \AA^{-1} . We suggest that this mode mixing is another route for producing low thermal conductivity as already pointed out^{29,47}.

In summary, we have presented a detailed comparison of the lattice dynamics of the icosahedral quasicrystal and its 1/1 approximant in the Zn-Sc system. As a result of the similar local environment and of the strong chemical order we observed a structured response function $S(\mathbf{Q},E)$ with distinct dispersionless broad optical excitations for both the QC and the approximant. We have evidenced a pseudo gap between an optical and the 2-fold transverse acoustic branch. A low lying dispersionless excitation is also observed around 6 meV in longitudinal geometry which might be related to the vibrational spectrum of the inner tetrahedron. Besides these similarities, significant differences have been observed. As a general trend, the pseudo gap is larger and better seen in the approximant than in the quasicrystal. This can be qualitatively explained by the occurrence of several PBZB in the QC whereas only one is present in the approximant. These observations are well reproduced by simulations using pair potential and realistic atomic models. Similarities and differences are clearly reproduced, both in the dispersion relation but also in the intensity distribution of the response function $S(\mathbf{Q},E)$. This paves the way for a detailed understanding of the physics of quasicrystals.

METHODS

Sample preparation

Single crystals of the 1/1 approximant and of the QC have been obtained by slow cooling from the melt using Bridgman or solution growth techniques. Elements were first encapsulated in Mo foils, and kept several hours in the liquid state. Large single grains have been extracted from the ingot for the purpose of inelastic neutron scattering experiments. Their single grain character has been checked by hard x-ray Laue topography which allows for the bulk of the sample to be probed⁴⁸. For neutron measurements we used two single grains quasicrystals: the first one, labelled hereafter i-ZnMgSc-A, has a volume of 0.1 cm^3 and a mosaic of the order 0.7° . The second sample, i-ZnMgSc-B, has a mosaic spread of 1.7° and a volume of 0.4 cm^3 . The i-ZnMgSc-A sample was used to measure accurately the low energy part of the acoustic branch. The crystal approximant has a mosaic of about 0.8° and a volume of 0.3 cm^3 . The same i-ZnMgSc-A sample was also used for inelastic x-ray scattering measurements. A smaller crystal approximant was used for inelastic x-ray measurements. The $100 \times 1000 \text{ \mu m}^2$ footprint size of the x-ray beam only probes a small volume of the sample for which we found a mosaic spread of the order 0.04° .

Inelastic neutron and X-ray scattering

Inelastic neutron scattering measurements have been carried out at the Orphee Reactor, Laboratoire Leon Brillouin (Saclay) on the 1T triple axis spectrometer. We used a vertically bent PG 002 monochromator and a doubly bent PG 002 analyser. A graphite filter was placed

in front of the analyser to suppress higher order harmonics. The spectrometer was operated in the constant $k_F=2.662 \text{ \AA}^{-1}$ scan procedure and we measured excitations in the range 0-16 meV. With the set up used the elastic energy resolution is of the order of 1.5 meV and has an almost Gaussian shape. The phonon instrumental resolution depends on the phonon energy, the dispersion relation and the sample mosaic. With a 0.7° sample mosaic and for TA phonon at 6 meV, the phonon instrumental resolution is of the order of 1.4 meV and it degrades for higher sample mosaic. We thus used the i-ZnMgSc-A sample for accurate determination low energy transverse acoustic excitations of the quasicrystal, whereas the larger sample i-ZnMgSc-B, was used to measure higher energy excitations. The data have been fitted using the *hfit* software, which convolves the modelled excitation with the instrumental resolution. Acoustic phonons have been modelled by a damped harmonic oscillator (DHO), whereas the optic-like excitations have been modelled by Gaussian distributions. Similarly to other QC studies, we found that the Gaussian distribution best reproduces the rather broad bands of optical excitations. Higher energy modes (between 16 and 30 meV) have been measured on the IN22 CRG instrument (ILL, Grenoble). We used the same configuration as the one of 1T. Most of the scan have been measured with a constant $k_F=2.662 \text{ \AA}^{-1}$.

Inelastic x-ray scattering measurements have been carried out on the BL35XU beamline of the SPring-8 synchrotron (Japan, proposal 2004A0439-ND3d-np). Beamline design and characteristics are described in ref.⁴⁹. We used a Si(11 11 11) monochromator and analyser, with an incoming X-ray energy of 21.75 keV. The beam was focused on the sample position with a size of about $100 \times 150 \text{ \mu m}^2$. The elastic resolution has a Lorentzian shape, with a FWHM of 1.8 meV. In order to extract properly the elastic contribution, we performed energy scans in the range of -10, +30 meV. As for the neutron results, acoustic phonons have been modelled by a DHO, whereas optic like excitations were modelled by Gaussian distributions, both convoluted by the instrumental resolution.

Normalised inelastic intensity

In the long wavelength limit, $|\mathbf{q}| \ll |\mathbf{Q}|$, and in the classical limit $E \ll k_B T$ one can define for both the periodic crystal and the QC a normalised intensity $I_N(E)$ for each acoustic mode by:

$$I_N(E) = E^2 \int S(\mathbf{Q}_{\text{Bragg}} + \mathbf{q}, E) dE \propto I_{\text{Bragg}} (\mathbf{Q} \cdot \mathbf{e}_s)^2 \quad (1)$$

In which I_{Bragg} is the Bragg peak intensity and \mathbf{e}_s is the doubly-degenerated transverse or longitudinal polarisation of the acoustic mode. When measuring an acoustic mode close to a strong Bragg peak, the normalised intensity is thus a constant as a function of \mathbf{q} as long as the dispersion is linear and the mode has an acoustic character. We used this relation to evidence the acoustic character of a mode.

Pair potentials fitting ab-initio data.

Our pair potentials fit a database of ab-initio calculated forces and energy differences, computed using the density-functional theory based code VASP⁵⁰. The database contained low-temperature as well as high-temperature samples of ScZn_{12} , ScZn_6 and ScZn_2

compounds. The pair potentials are expressed by an analytical oscillating form¹⁶, fitting accurately the ab-initio force and energy difference data points by 6 parameters per each of the three pairs Sc-Sc, Sc-Zn and Zn-Zn. The fitted potentials are shown in Fig. 6.

References

1. Shechtman, D., Blech, I., Gratias, D. & Cahn, J. W. Metallic phase with long-range orientational order and no translational symmetry. *Phys. Rev. Lett.* **53**, 1951-1953 (1984).
2. Tsai, A. P., Guo, J. Q., Abe, E., Takakura, H. & Sato, T. J. A stable binary quasicrystal. *Nature* **408**, 537-538 (2000).
3. Kaneko, Y., Arichika, Y. & Ishimasa, T. Icosahedral quasicrystal in annealed Zn-Mg-Sc alloys. *Phil. Mag. Lett.* **81**, 777-87 (2001).
4. Gomez, C. P. & Lidin, S. Structure of Ca₁₃Cd₇₆ : A Novel Approximant to the MCd_{5.7} Quasicrystals (M.Ca, Yb). *Angew. Chem. Int.* **40**, 4037-39 (2001).
5. Gomez, C. P. & Lidin, S. Comparative structural study of the disordered MCd/sub 6/ quasicrystal approximants. *Phys. Rev. B* **68**, 024203\1-9 (2003).
6. Takakura, H., Gomez, C. P., Yamamoto, A., de Boissieu, M. & Tsai, A. P. Atomic structure of the binary icosahedral Yb-Cd quasicrystal. *Nature Materials* **6**, 58-63 (2007).
7. Janssen, T., Chapuis, G. & de Boissieu, M. *Aperiodic Crystals. From modulated phases to quasicrystals* (Oxford University Press, Oxford, 2007).
8. Fujiwara, T. & Ishii, Y. *Physics of Quasicrystals* (Elsevier Science, 2007 (in press)).
9. Hasegawa, J., Tamura, R., Takeuchi, S., Tokiwa, K. & Watanabe, T. Electronic transport of the icosahedral Zn-Mg-Sc quasicrystal and its 2/1 and 1/1 cubic approximants. *J. of Non-Crystalline Sol.* **334**, 368-371 (2004).
10. Kuo, Y. K., Lai, J. R., Huang, C. H., Ku, W. C., Lue, C. S. & Lin, S. T. Thermoelectric properties of binary Cd-Yb quasicrystals and Cd₆Yb. *J. Appl. Phys.* **95**, 1900-1905 (2004).
11. Kuo, Y. K., Sivakumar, K. M., Lai, H. H., Ku, C. N., Lin, S. T. & Kaiser, A. B. Thermal and electrical transport properties of Ag-In-Yb quasicrystals: An experimental study. *Phys. Rev. B* **72** (2005).
12. Tamura, R., Murao, Y., Kishino, S., Takeuchi, S., Tokiwa, K. & Watanabe, T. Electrical properties of the binary icosahedral quasicrystal and its approximant in the Cd-Yb system. *Mater. Sci. Eng.* **375-77**, 1002-1005 (2004).
13. Tamura, R., Murao, Y., Takeuchi, S., Kiss, T., Yokoya, T. & Shin, S. Comparative study of the binary icosahedral quasicrystal Cd_{5.7}Yb and its crystalline approximant Cd₆Yb by low-temperature ultrahigh-resolution photoemission spectroscopy. *Phys. Rev. B* **65** (2002).
14. Tamura, R., Takeuchi, T., Aoki, C., Takeuchi, S., Kiss, T., Yokoya, T. & Shin, S. Experimental evidence for the p-d hybridization in the Cd-Ca quasicrystal: Origin of the pseudogap. *Phys. Rev. Lett.* **92** (2004).
15. Tamura, R., Araki, T. & Takeuchi, S. Is the negative temperature coefficient of the resistivity of the quasicrystals due to chemical disorder? *Phys. Rev. Lett.* **90** (2003).
16. Mihalkovic, M., Henley, C. L., Widom, M. & Panchapakesan, G. Accurate pair potentials for alloys from ab-initio fits. *Submitted* (2007).
17. de Boissieu, M., Francoual, S., Kaneko, Y. & Ishimasa, T. Diffuse Scattering and phason fluctuations in the Zn-Mg-Sc icosahedral quasicrystal and its Zn-Sc periodic approximant. *Phys. Rev. Lett.* **95**, 105503\1-4 (2005).

18. Ishii, Y. & Fujiwara, T. Hybridization mechanism for cohesion of Cd-based quasicrystals. *Phys. Rev. Lett.* **87**(20), 206408/1-4 (2001).
19. Quilichini, M. & Janssen, T. Phonons in quasicrystals. *Rev. Mod. Phys.* **69**, 277 (1997).
20. Smith, A. P. & Ashcroft, N. W. Pseudopotentials and quasicrystals. *Phys. Rev. Lett.* **59**(12), 1365-1368 (1987).
21. Lu, J. P. & Birman, J. Acoustic-wave propagation in quasiperiodic, incommensurate, and random systems. *Phys. Rev. B* **38**(12), 8067-8074 (1988).
22. Niizeki, K. & Akamuatsu, T. The reciprocal space properties of the electronic wave functions of the Penrose lattice. *Journal of Physics: Condensed Matter* **2**(33), 7043-7047 (1990).
23. Niizeki, K. & Akamatsu, T. Special points in the reciprocal space of an icosahedral quasi-crystal and the quasi-dispersion relation of electrons. *J. Phys.: Cond. Matter* **2**(12), 2759-2771 (1990).
24. Quilichini, M., Heger, G., Hennion, B., Lefebvre, S. & Quivy, A. Inelastic neutron scattering study of acoustic modes in a monodomain AlCuFe quasicrystal. *J. Phys. France* **51**, 1785-1790 (1990).
25. Goldman, A. I., Stassis, C., de Boissieu, M., Currat, R., Janot, C., Bellissent, R., Mouden, H. & Gayle, F. W. Phonons in icosahedral and cubic Al-Li-Cu. *Phys. Rev. B* **45**, 10280-10291 (1992).
26. de Boissieu, M., Boudard, M., Bellissent, R., Quilichini, M., Hennion, B., Currat, R., Goldman, A. I. & Janot, C. Dynamics of the AlPdMn Icosahedral Phase. *J Phys: Condens Matter* **5**, 4945-4966 (1993).
27. Boudard, M., de Boissieu, M., Kycia, S., Goldman, A. I., Hennion, B., Bellissent, R., Quilichini, M., Currat, R. & Janot, C. Optic modes in the AlPdMn icosahedral phase. *J. Phys.: Condens. Matter* **7**, 7299-7308 (1995).
28. Shibata, K., Currat, R., de-Boissieu, M., Sato, T. J., Takakura, H. & Tsai, A. P. Dynamics of the ZnMgY icosahedral phase. *Journal of Physics: Condensed Matter* **14**, 1847-63 (2002).
29. de Boissieu, M., Currat, R., Francoual, S. & Kats, E. Sound-mode broadening in quasicrystals: a simple phenomenological model. *Phys. Rev. B* **69**(5), 54205-1-8 (2004).
30. Cahn, J. W., Shechtman, D. & Gratias, D. Indexing of icosahedral quasiperiodic crystals. *J. Mat. Res.* **1**, 13-26 (1986).
31. Benoit, C., Poussiguet, G. & Azougarh, A. Neutron scattering by phonons in quasi-crystals. *J. Phys. : Cond. Matter* **2**, 2519-2536 (1990).
32. Tamura, R., Nishimoto, K., Takeuchi, S., Edagawa, K., Isobe, M. & Ueda, Y. Universal low-temperature phase transition in Zn- and Cd-based crystalline approximants. *Phys. Rev. B* **71**, 092203-1 -4 (2005).
33. Ishimasa, T., Kasano, Y., Tachibana, A., Kashimoto, S. & Osaka, K. Low temperature phase of the Zn-Sc approximant. *Phil. Mag.* **87**, 2887-2897 (2007).
34. Lin, Q. S. & Corbett, J. D. The 1/1 and 2/1 approximants in the ScMgZn quasicrystal system: Triacanthedral clusters as fundamental building blocks. *Journal of the American Chemical Society* **128**, 13268-13273 (2006).
35. Henley, C. L. Cell geometry for cluster-based quasicrystal models. *Phys. Rev. B* **43**, 993-1020 (1991).
36. Mihalkovic, M. & Widom, M. Canonical cell model of cadmium-based icosahedral alloys. *Phil. Mag.* **86**, 519-527 (2006).
37. Rog, T., Murzyn, K., Hinsen, K. & Kneller, G. R. A Program Package for a Neutron Scattering Oriented Analysis of Molecular Dynamics Simulations. *J. Comput. Chem.* **24**, 657-667 (2003).
38. Janot, C. & de-Boissieu, M. Quasicrystals as a hierarchy of clusters. *Phys. Rev. Lett.* **72**, 1674-7 (1994).
39. Duval, E., Saviot, L., Mermet, A. & Murray, D. B. Continuum elastic sphere vibrations as a model for low lying optical modes in icosahedral quasicrystals. *J. Physics: Cond. Matter* **17**, 3559-65 (2005).

40. Janot, C. Conductivity in quasicrystals via hierarchically variable-range hopping. *Phys. Rev. B*, 181-91 (1996).
41. Zoorob, M. E., Charlton, M. D. B., Parker, G. J., Baumberg, J. J. & Netti, M. C. Complete photonic bandgaps in 12-fold symmetric quasicrystals. *Nature* **404**, 740-743 (2000).
42. Lai, Y., Zhang, X. D. & Zhang, Z. Q. Large sonic band gaps in 12-fold quasicrystals. *Journal of Applied Physics* **91**, 6191-6193 (2002).
43. Sales, B. C., Mandrus, D., Chakoumakos, B. C., Keppens, V. & Thompson, J. R. Filled skutterudite antimonides: Electron crystals and phonon glasses. *Physical Review B* **56**, 15081-15089 (1997).
44. Chernikov, M. A., Bianchi, A. & Ott, H. R. Low-Temperature Thermal-Conductivity of Icosahedral Al₇₀Mn₉Pd₂₁. *Physical Review B* **51**, 153-158 (1995).
45. Smontara, A., Smiljanic, Bilusic, A., Grushko, B., Balanetsky, S., Jaglici, Z., Vrtnik, S. & Dolinsek, J. Complex Epsilon-phases in the Al-Pd-transition-metal systems: Towards a combination of an electrical conductor with a thermal insulator. *J. Alloys Compd.*, In press (2007).
46. Kalugin, P. A., Chernikov, M. A., Bianchi, A. & Ott, H. R. Structural scattering of phonons in quasicrystals. *Physical Review B* **53**, 14145-14151 (1996).
47. Takeuchi, T., Nagasako, N., Asahi, R. & Mizutani, U. Extremely small thermal conductivity of the Al-based Mackay-type 1/1-cubic approximants. *Physical Review B* **74** (2006).
48. Hamelin, B. & Bastie, P. A new hard X-ray diffractometer (100-400 keV) for bulk crystalline analysis. Applications for non-destructive investigation. *Proceedings of SPIE*, 29-39 (2002).
49. Baron, A. Q. R., Tanaka, Y., Goto, S., Takeshita, K., Matsushita, T. & Ishikawa, T. An X-Ray Scattering Beamline for Studying Dynamics. *Journal of Physics and Chemistry of Solids* **61**, 461-465 (2000).
50. Kresse, G. & Furthmuller, J. Efficient iterative schemes for ab initio total-energy calculations using a plane-wave basis set. *Physical Review B* **54**, 11169-11186 (1996).

Acknowledgments

We acknowledge the LLB, the ILL and the Spring-8 facilities for the allocation of beam time. We thank Y. Kaneko for his help in sample preparation. Part of the work has been initiated within the European Complex Metallic Alloy network of excellence. M. M. has been supported by a CNRS grant during his stay at the SIMAP, and by the Slovak grant agency APVV-0413-06. M. dB acknowledges the financial support of the Tohoku University during his stay at the IMRAM. Correspondence and requests for materials should be addressed to Marc de Boissieu.

FIGURE CAPTIONS

Figure 1: Cluster structure and diffraction pattern of the i-ZnMgSc quasicrystal and its 1/1 Zn-Sc approximant.

(a) The successive shells forming the triacontahedral cluster observed in both the 1/1 approximant and the quasicrystal. First a Zn tetrahedron (disordered), then a Zn dodecahedron followed by a Sc icosahedron, then a Zn icosidodecahedron and finally a Zn triacontahedron with atoms on vertices and mid-edges. The 1/1 approximant is a BCC packing of the cluster, whereas they are packed quasiperiodically in the quasicrystal. Positions of Mg atoms have not been determined in the QC. Arrows illustrates the deviation from icosahedral symmetry of the icosidodecahedron: the 2 triangular faces have not the same size.

(b) and (c) 2-fold diffraction pattern of the 1/1 Zn-Sc approximant and of the i-ZnMgSc quasicrystal. The area of the dots is proportional to the intensity of the corresponding Bragg peaks, A few indices are indicated. Measurements have been carried out mainly around the (10,0,0) and 52/84x Bragg peaks.

Figure 2: Response function measured in transverse geometry by inelastic neutron scattering for the ZnSc 1/1 approximant and the ZnMgSc QC.

The figure displays the intensity distribution of the $S(Q, E)$ measured function. The threshold has been set to allow the visualisation of low intensity optical excitations. The dispersion relation extracted from the data is superimposed on the colour figure. The vertical white lines indicate the (pseudo) Brillouin zone boundaries, and the dark vertical line is for the zone centre (10,2,0). In the acoustic regime, circles indicate a constant normalised intensity, whereas triangles indicate an increase in the normalised intensity. The linear dispersion in the acoustic regime is indicated with a continuous line.

Figure 3. Longitudinal excitations: comparison between the measured dispersion relation (symbols) and the simulated response function $S(Q,E)$ (temperature colour-coded) in the 1/1 approximant (left panel) and the quasicrystal (right panel). Symbols correspond to the position of the excitations extracted from the inelastic X-ray spectrum. The black full circles and triangles stand for the acoustic signal whereas other symbols correspond to optical excitations. Black triangles indicate the q positions for which the normalised acoustic intensity is no longer constant. The experimental dispersion relations are superimposed on the simulated intensity distribution shown as a temperature colour-coded scale. The vertical dashed white lines indicate the position of the (pseudo) Brillouin zone boundaries.

Figure 4: Transverse excitations: comparison between the measured dispersion relation (symbols) and the simulated response function $S(Q,E)$ (temperature colour-coded) in the 1/1 approximant (left panel) and the quasicrystal (right panel). The figure shows the intensity distribution of the simulated response function on a temperature colour-coded scale. The scattering geometry is the same as in figure 2. The experimental positions of the excitations, as measured by neutron inelastic scattering, are shown by symbols: the black closed circles and triangles stand for the acoustic signal whereas other symbols correspond to optical excitations. Black triangles indicate the q positions for which the normalised acoustic

intensity is no longer constant. Vertical white dashed lines indicate the position of the (pseudo) Brillouin zone boundaries. The simulation reproduces both the general trend and the differences observed between the QC and its approximant.

Figure 5: Comparison between the experiment and the simulation for a few representative constant Q energy scans. Circles correspond to the measurement, red lines are fit to the data (from which dispersion relations are extracted), blue lines show the simulated response function $S(Q, E)$. The q value is indicated in insert. Left panels: transverse acoustic modes measured in the 1/1 approximant and the quasicrystal by inelastic neutron scattering. Right panels: longitudinal excitations measured in the 1/1 approximant and quasicrystal by inelastic X-ray scattering (For clarity the elastic contribution has been subtracted from the data). The simulated data have been convoluted by a Gaussian with a FWHM of 1 meV and 3 meV for neutron and X-ray data respectively. The energy position of the two transverse calculated spectra at 0.18 \AA^{-1} have been artificially translated at higher energy in order to illustrate the good reproduction of excitation whose width is limited by the instrumental resolution. Notice the visible broadening, as q increases in transverse geometry. The intensity distribution is well reproduced by the simulation. Note in particular the good reproduction of the longitudinal scans at $+ \text{ or } - 0.43 \text{ \AA}^{-1}$. Red arrows point to remarkable similarities and differences (see text).

Figure 6: Fitted pair potential used in the simulation. The blue, red and black lines stand for Zn-Zn, Sc-Sc and Zn-Sc pair potential. Note the oscillating part, reminiscent of Friedel like oscillations. As expected from the large atomic size differences the Zn-Zn potential has a first (shallow) minimum located at 2.85 \AA whereas the Sc-Sc's potential is located at 3.34 \AA .

FIGURE 1

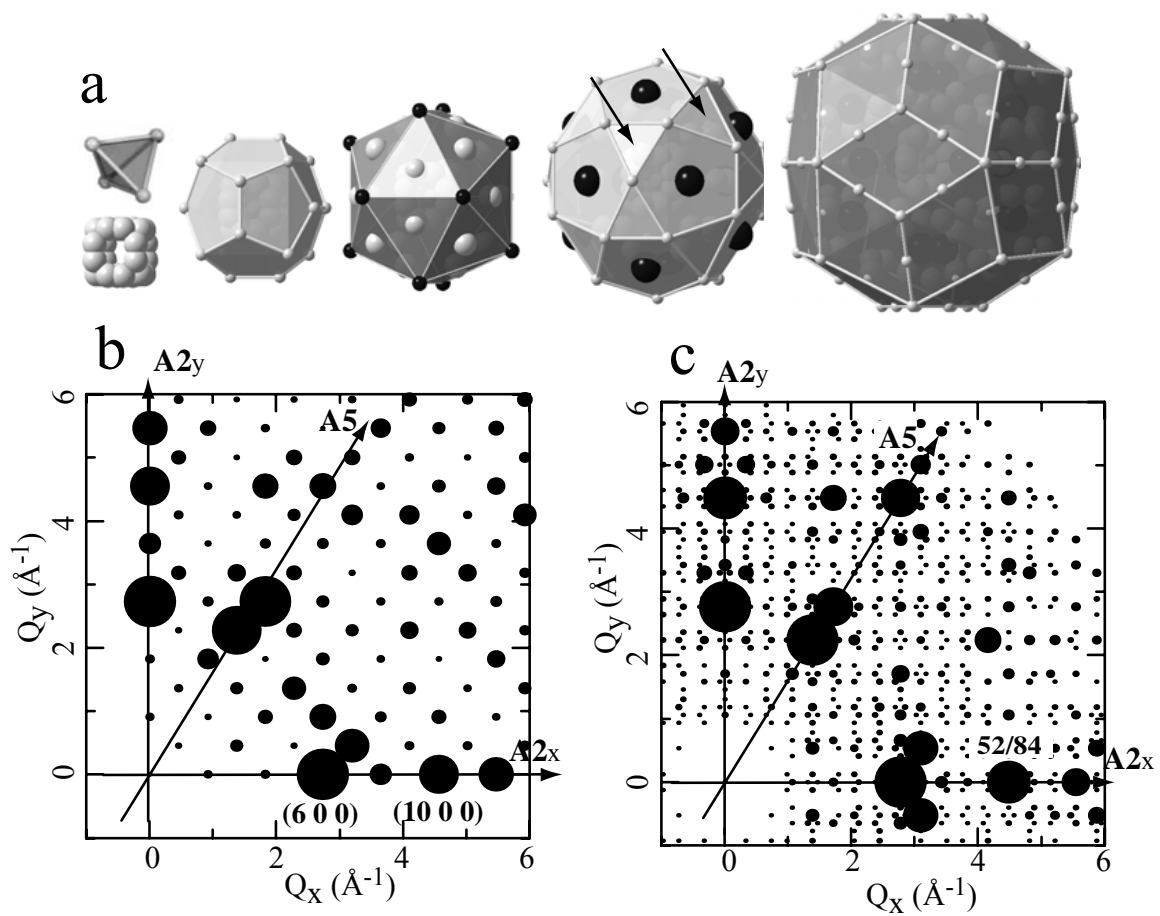
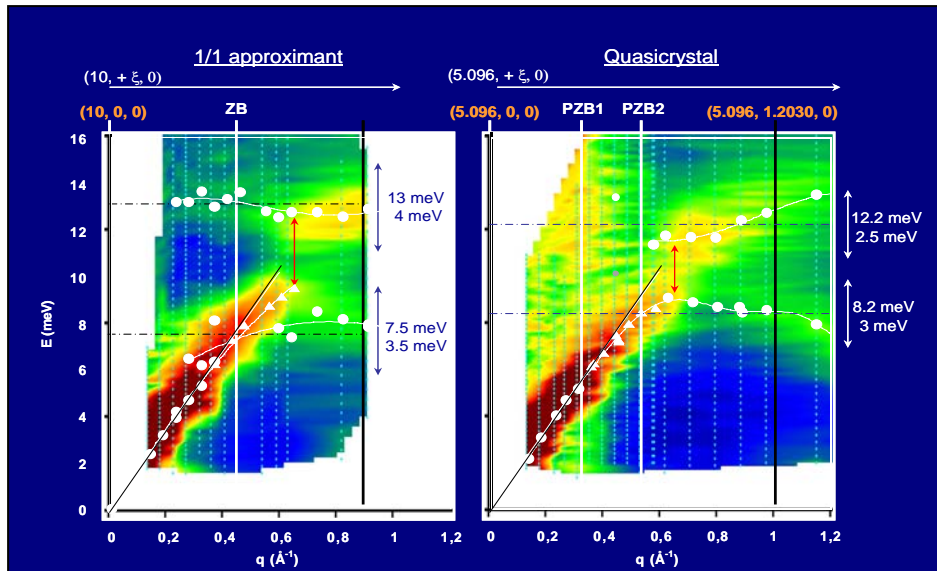


FIGURE 2



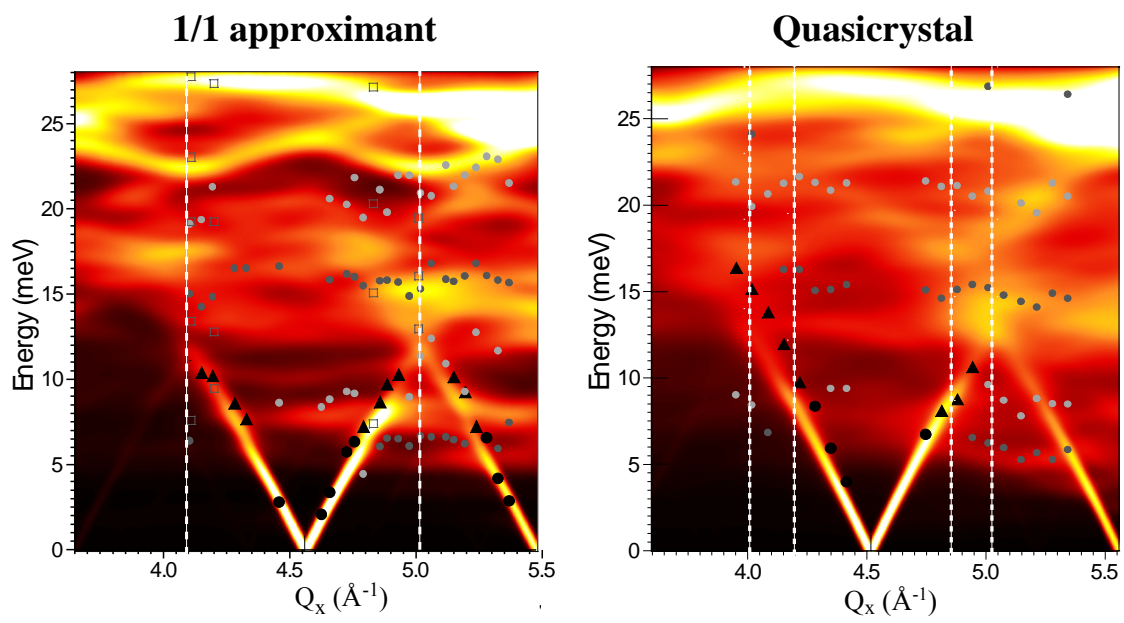


FIGURE 3:

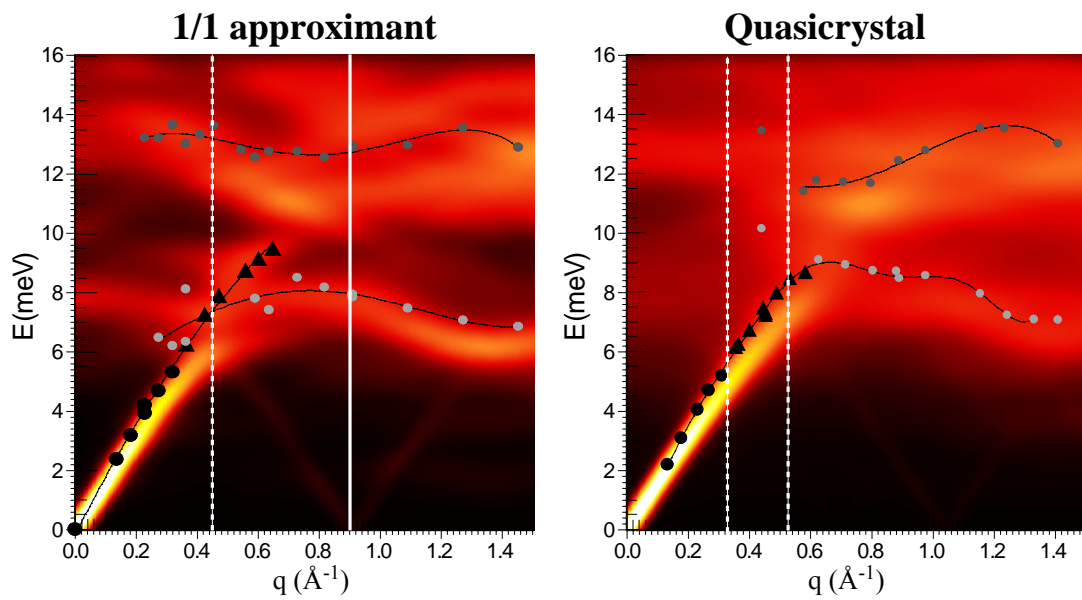
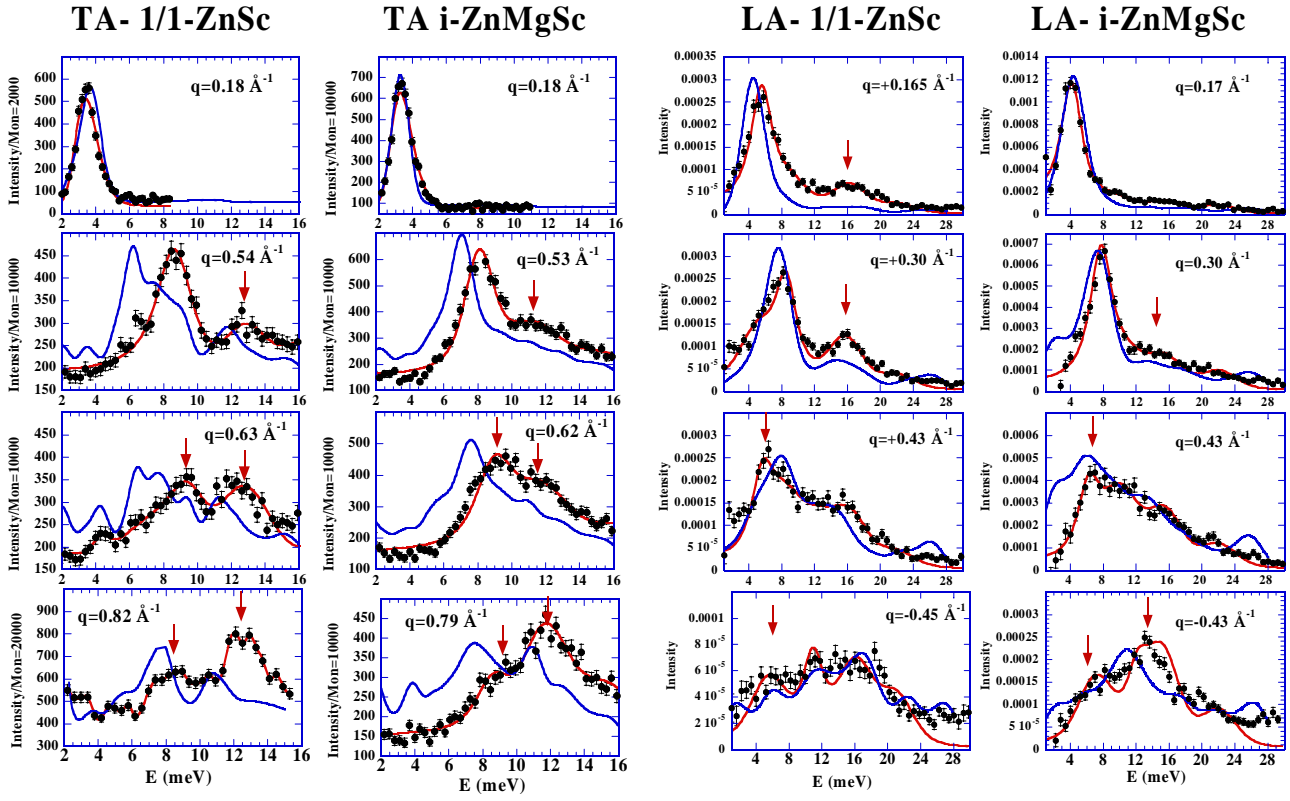


FIGURE 4:

FIGURE 5:



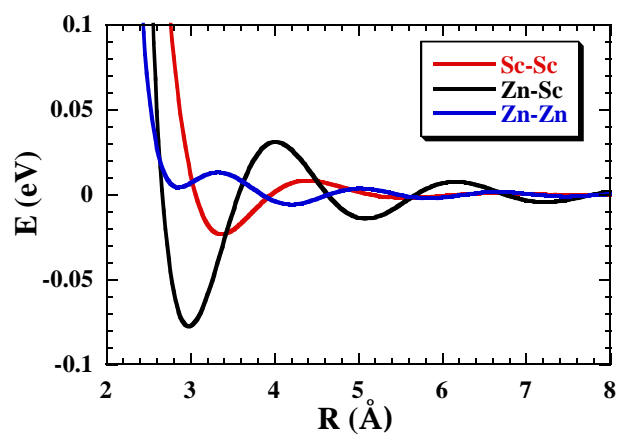


Figure 6